

# A numerical study of gravity-driven instability in strongly coupled dusty plasma. Part 3. Homo-interaction between a pair of rising/falling bubbles/droplets

Vikram S. Dharodi  

Department of Physics and Astronomy, West Virginia University, Morgantown, WV 26506, USA

(Received 19 May 2024; revised 26 August 2024; accepted 28 August 2024)

A numerical study of the homo-interactions between two falling droplets and between two rising bubbles in a strongly coupled dusty plasma medium is presented in this article. The strongly coupled dusty plasma is considered as a viscoelastic fluid using the generalized hydrodynamic fluid model formalism. Two factors that affect homo-interactions are taken into account: the initial spacing and the coupling strength of the medium. Three different spacings between two droplets are simulated: widely, medium and closely. In each case, the coupling strength has been given as mild–strong and strong. It is shown that the overall dynamic is governed by the competition between the acceleration of two droplets/bubbles due to gravity and the interaction due to the closeness of the droplets/bubbles. Particularly in viscoelastic fluids, apart from the initial separation, shear waves originating from rotating vortices are responsible for the closeness of two droplets or bubbles. Several two-dimensional simulations have been carried out. This work is a continuation of the work done in Parts 1 (Dharodi & Das, *J. Plasma Phys.*, vol. 87, issue 2, 2021, 905870216) and 2 (Dharodi, *J. Plasma Phys.*, vol. 87, issue 4, 2021, 905870402).

**Key words:** dusty plasmas, complex plasmas, plasma instabilities

---

## 1. Introduction

The buoyancy instability, which is driven by gravity, is what makes an object sink or float in a fluid. A droplet sinks into the fluid in the direction of gravity, whereas a bubble defies gravity and rises to the surface. Bubbles and droplets are frequently observed in a variety of fields, such as engineering, biomedical, agricultural, industrial and environmental (Bourouiba & Bush 2012; Jia & Zhu 2015; Zhao *et al.* 2017; Moghtadernejad, Lee & Jadidi 2020; Aliabouzar *et al.* 2023; Wang *et al.* 2023). From fundamental perspective of physics, droplets and bubbles play a significant role in transportation across any medium, for example, heat exchange, diffusion, mixing, etc. Understanding the interaction between bubbles and droplets is therefore essential to comprehending how the flow field evolves. Bubbles and droplets have been studied separately and together in different media (Mokhtarzadeh-Dehghan & El-Shirbini 1985; Dwyer 1989; Cristini & Tan 2004; Shew & Pinton 2006; Chen *et al.* 2008; Zhu, Sui &

† Email address for correspondence: [vikram.ipr@gmail.com](mailto:vikram.ipr@gmail.com)

Djilali 2008; Tabor *et al.* 2011; Gaudron, Warnez & Johnsen 2015; Dollet, Marmottant & Garbin 2019; Leong & Le 2020).

Numerical simulations and experiments have been carried out recently to study the interactions between two bubbles rising side by side in viscous liquids (Kong *et al.* 2019; Zhang, Chen & Ni 2019). Using atomic force microscopy, the homo- and hetero-interactions between oil droplets and air bubbles are assessed by Tabor *et al.* (2011). In order to study the plasma–liquid interaction, water droplet evolution in a plasma medium and underwater discharge in the bubbles have been studied by Oinuma *et al.* (2020) and Tachibana *et al.* (2011), respectively. In plasmas, studies of bubbles and/or droplets under different circumstances have been carried out (Arzhannikov *et al.* 2013; Wang *et al.* 2015; Ning *et al.* 2021; Ou, Brochard & Morgan 2021). Stenzel & Urrutia (2012*a,b,c,d*) conducted a series of experiments on oscillating plasma bubbles, where bubbles are produced by introducing a negatively biased grid into the surrounding plasma. A laboratory dusty plasma is a good illustration of a homogeneous plasma; however, density fluctuations may be created using laser pulses and external forces like magnetic and/or electric, size or charge imbalance, etc. These density fluctuations can be associated with bubble and/or droplet conditions. Chu *et al.* (2003) and Teng *et al.* (2008) have explored the dynamics of pulsed laser-induced travelling microbubbles in dusty plasma, and Chen, Chu & Lin (2006) have explored them in a thin ink sheet between two glass slices. In a dusty plasma, under the effect of thermophoresis, Schwabe *et al.* (2009) have reported the spontaneous creation of bubbles, drops, and spraying cusps.

Two regions have been added, one high density and the other low density, to form a droplet and a bubble in the background medium, respectively. In Part 1 (Dharodi & Das 2021) of this series, the individual dynamics of a rising bubble and a falling droplet have been explored, and in Part 2 (Dharodi 2021), the hetero- (bubble-droplet) interactions between a rising bubble and a falling droplet have been studied. For these studies, the dusty plasma is taken into consideration as a medium. The study of dust is important from the perspective of both industrial (Melzer *et al.* 2000; Merlino & Goree 2004; Chaubey & Goree 2023*a,b*; Ramkorun *et al.* 2024*a,b*) and fundamental physics (Choudhary, Mukherjee & Bandyopadhyay 2016, 2017, 2018; Dharodi & Kostadinova 2023; Kumar *et al.* 2023). Dusty plasma is gravitationally favourable due to the high mass of dust grains and readily forms a strong coupling regime caused by the high charge of the dust grains. Therefore, the strongly coupled dusty plasma (SCDP) can serve as a perfect medium to study the role of strong coupling on the growth of gravity-driven instability like buoyancy. A SCDP behaves similarly to a viscoelastic (VE) fluid below the crystallization limit (Ikezi 1986; Vladimirov, Shevchenko & Cramer 1997).

Here, to simulate the SCDP as a VE fluid, a well-known phenomenological generalized hydrodynamics (GHD) fluid model (Kaw & Sen 1998; Kaw 2001) has been implemented. This model characterizes the VE effects through two coupling parameters: shear viscosity  $\eta$  and the Maxwell relaxation parameter  $\tau_m$  (Frenkel 1955). Due to the strong correlation between dust grains, the viscosity  $\eta$  in the presence of elasticity  $\tau_m$  contributes to the transverse mode. The incompressible limit of the GHD model (i-GHD) has been considered to investigate the exclusive effect of transverse modes and to prevent a possible coupling with the longitudinal model. The transverse modes in the dusty plasma medium have been investigated by computational (Schmidt *et al.* 1997), experimental (Nunomura, Samsonov & Goree 2000; Pramanik *et al.* 2002) and analytical (Peeters & Wu 1987; Vladimirov *et al.* 1997; Wang, Bhattacharjee & Hu 2001) methods. Using the i-GHD model, computationally, the transverse shear (TS) modes and their role in various physical processes have been explored (Das, Dharodi & Tiwari 2014; Dharodi, Tiwari & Das 2014; Tiwari *et al.* 2014*a,b*, 2015; Dharodi 2016; Dharodi *et al.* 2016; Dharodi 2020;

Dharodi, Patel & Das 2022; Dharodi & Kostadinova 2024). Employing the same model, the current work explores how the coupling strength of the background VE fluid affects the homo-interactions between two falling droplets and between two rising bubbles. The idea of homo-interaction was proposed in Part 2. In order to analyse phenomena at the dust time scale, one can disregard the fast response of lighter electrons and lighter ions. The balance between pressure and electric field results in the Boltzmann distribution of electron and ion densities. Dust continuity and momentum, along with Poisson's equation, constitute the governing set of equations for the dust dynamics.

Three different spacings between two droplets are simulated: widely, medium and closely. In each case, the coupling strength has been presented as mild-strong ( $\eta = 2.5$ ,  $\tau_m = 20$ ) and strong ( $\eta = 2.5$ ,  $\tau_m = 10$ ). These are comparable to regimes that can be attained in laboratory settings. For example, in Feng, Goree & Liu (2012), a range of frequency-dependent normalized viscosity values  $\eta = 0.1$ – $0.5$  and a normalized relaxation time  $\tau_m = 3$  were obtained using data from studies with dusty plasma monolayers. Using the dimensionless values for  $\tau_m$  and  $\eta$ , we estimate that a range of ratios relevant to this experiment is  $\eta/\tau_m = 0.03$ – $0.16$ , which is covered by the mild–strong case in our simulations. Since the behaviour of two falling droplets is similar to the behaviour of two rising bubbles, mainly the droplet case will be discussed. For widely spaced, unlike classical, hydrodynamic (HD) fluids, it is found that shear waves in VE fluids facilitate the pairing between two bubbles/droplets. In the case of medium spacing, the two new dipoles of unequal strength blobs exhibit a circular motion and exchange their partners. For close spacing, the droplet/bubble fall/rise is suppressed as the medium's coupling strength increases. This work may have significant applications in plasmas where density heterogeneity exists in the presence of shear waves. The dynamics of bubbles and/or droplets in electron–ion plasmas, in the presence of shear waves, may be governed by external forces such as electric and/or magnetic forces rather than gravity. Whereas gravity becomes important in dusty plasmas.

This paper is organized in the following sections. The next § 2 describes the basic model equations and the implementation of our numerical scheme. In § 3, simulation results have been reported. The role of coupling strength on falling of droplet–droplet and rising of bubble–bubble density dynamics has been depicted in the form of TS waves through corresponding vorticity contour plots. To develop a better physical insight into the dynamics of each phenomenon, the inviscid limit of HD fluids is also simulated for each case. Finally, § 4, concludes the paper with a summary.

## 2. The numerical model and simulation methodology

For a dusty plasma under gravity acceleration  $\mathbf{g}$ , the generalized hydrodynamic fluid model is given by a coupled set of continuity and momentum equations (Kaw & Sen 1998)

$$\frac{\partial \rho_d}{\partial t} + \nabla \cdot (\rho_d \mathbf{v}_d) = 0, \quad (2.1)$$

$$\left[ 1 + \tau_m \left( \frac{\partial}{\partial t} + \mathbf{v}_d \cdot \nabla \right) \right] \left[ \rho_d \left( \frac{\partial \mathbf{v}_d}{\partial t} + \mathbf{v}_d \cdot \nabla \mathbf{v}_d \right) + \rho_d \mathbf{g} + \rho_c \nabla \phi_d \right] = \eta \nabla^2 \mathbf{v}_d, \quad (2.2)$$

respectively, and the incompressible condition is given as

$$\nabla \cdot \mathbf{v}_d = 0. \quad (2.3)$$

When thinking about disturbances in the medium whose propagation is significantly slower than the speed of sound, incompressibility is always a suitable approximation. This

model describes a basic hydrodynamic fluid in the limit  $\tau_m=0$  through the Navier–Stokes equation. The derivation of these normalized equations, as well as the procedure for their numerical implementation and validation, have been thoroughly discussed in earlier works (Dharodi *et al.* 2014, 2016). Here, the number density of the dust fluid is  $n_d$ , the mass of the dust particle is  $m_d$  and the mass density of the dust fluid is  $\rho_d = n_d m_d$ . The variables  $\rho_c$ ,  $\mathbf{v}_d$  and  $\phi_d$ , respectively, indicate the dust charge density, dust charge potential and dust fluid velocity. The time, length, velocity and potential are normalized using inverses of the dust plasma frequency  $\omega_{pd}^{-1} = (4\pi(Z_d e)^2 n_{d0}/m_d)^{-1/2}$ , plasma Debye length  $\lambda_d = (K_B T_i/4\pi Z_d n_{d0} e^2)^{1/2}$ ,  $\lambda_d \omega_{pd}$  and  $Z_d e/K_B T_i$ , respectively. The parameters  $m_d$ ,  $T_i$  and  $K_B$  stand for the dust grain mass, ion temperature and Boltzmann constant, respectively. The number density  $n_d$  is normalized by the equilibrium value  $n_{d0}$ . A constant charge on each dust grain has been taken,  $Z_d$ , which may be positive or negative. Dust particles are generally negatively charged, but in some circumstances – such as secondary electron emission (Shukla & Mamun 2015) or afterglow plasma conditions – they can acquire a positive charge (Chaubey *et al.* 2021; Chaubey & Goree 2022a,b, 2024).

### 2.1. Simulation methodology

For the numerical modelling the above generalized momentum equation (2.2) is transformed into a set of two coupled equations

$$\rho_d \left( \frac{\partial \mathbf{v}_d}{\partial t} + \mathbf{v}_d \cdot \nabla \mathbf{v}_d \right) + \rho_d \mathbf{g} + \rho_c \nabla \phi_d = \boldsymbol{\psi}, \quad (2.4)$$

$$\frac{\partial \boldsymbol{\psi}}{\partial t} + \mathbf{v}_d \cdot \nabla \boldsymbol{\psi} = \frac{\eta}{\tau_m} \nabla^2 \mathbf{v}_d - \frac{\boldsymbol{\psi}}{\tau_m}. \quad (2.5)$$

The quantity  $\boldsymbol{\psi}(x, y)$  represents the strain produced in the elastic medium by the time-varying velocity fields. It is supposed that there is no beginning flow and the density gradient and potential gradient are taken along the  $y$ -axis. In opposition to the fluid density gradient, the acceleration  $\mathbf{g}$  is applied. With small perturbations; density, scalar potential and dust velocity can be written as  $\rho_d(x, y, t) = \rho_{d0}(y, t = 0) + \rho_{d1}(x, y, t)$ ,  $\phi_d(x, y, t) = \phi_{d0}(y, t = 0) + \phi_{d1}(x, y, t)$  and  $\mathbf{v}_d(x, y, t) = 0 + \mathbf{v}_{d1}(x, y, t)$ , respectively. Under the equilibrium condition,  $\rho_{d0} \mathbf{g} = -\rho_c \partial \phi_{d0} / \partial y$ , rewrite (2.4) using the perturbations.

$$\frac{\partial \mathbf{v}_d}{\partial t} + \mathbf{v}_d \cdot \nabla \mathbf{v}_d + \frac{\rho_{d1}}{\rho_d} \mathbf{g} + \frac{\rho_c}{\rho_d} \nabla \phi_{d1} = \frac{\boldsymbol{\psi}}{\rho_d}. \quad (2.6)$$

The Boussinesq approximation ( $\rho_{d0} \gg \rho_{d1}$ ) and the curl of (2.6) are used to get

$$\frac{\partial \xi_z}{\partial t} + (\mathbf{v}_d \cdot \nabla) \xi_z = \frac{1}{\rho_{d0}} \nabla \times \rho_{d1} \mathbf{g} + \nabla \times \frac{\boldsymbol{\psi}}{\rho_d}. \quad (2.7)$$

Since a constant charge medium has been considered,  $\nabla \times \nabla \phi_{d1} = 0$ . Here, the vorticity  $\xi_z(x, y) = \nabla \times \mathbf{v}_d(x, y)$  is normalized with dust plasma frequency. The final numerical

model equations in term of variables  $x$  and  $y$  become

$$\frac{\partial \rho_d}{\partial t} + (\mathbf{v}_d \cdot \nabla) \rho_d = 0, \quad (2.8)$$

$$\frac{\partial \psi}{\partial t} + (\mathbf{v}_d \cdot \nabla) \psi = \frac{\eta}{\tau_m} \nabla^2 \mathbf{v}_d - \frac{\psi}{\tau_m}, \quad (2.9)$$

$$\frac{\partial \xi_z}{\partial t} + (\mathbf{v}_d \cdot \nabla) \xi_z = -\frac{g}{\rho_{d0}} \frac{\partial \rho_{d1}}{\partial x} + \frac{\partial}{\partial x} \left( \frac{\psi_y}{\rho_d} \right) - \frac{\partial}{\partial y} \left( \frac{\psi_x}{\rho_d} \right). \quad (2.10)$$

The set of the last three coupled equations has been solved numerically using the LCPFCT software (Boris *et al.* 1993). To update the velocity at each time step, the velocity–vorticity relation  $\nabla^2 \mathbf{v}_d = -\nabla \times \boldsymbol{\xi}$  is solved using a Poisson equation solver (FISPACK Swarztrauber, Sweet & Adams 1999) within LCPFCT. Boundary conditions in simulation studies are non-periodic along the vertical ( $y$ -axis) direction, but periodic in the horizontal ( $x$ -axis). To ensure grid independence of the numerical results in each example, a grid convergence analysis was conducted. In the HD limit i.e.  $\tau_m = 0$ , the vorticity equation (2.9) becomes

$$\frac{\partial \xi_z}{\partial t} + (\mathbf{v}_d \cdot \nabla) \xi_z = -\frac{g}{\rho_{d0}} \frac{\partial \rho_{d1}}{\partial x} + \eta \nabla^2 \xi_z. \quad (2.11)$$

Therefore, the set of (2.8) and (2.11) has been numerically solved for pure HD situations. Using the previously mentioned velocity–vorticity relationship, the fluid velocity at each time step is updated. The first term on the left-hand side of (2.10) and (2.11) includes both gravity and the density gradient, which suggests that the density gradient in the presence of gravity assists the development of gravity-driven instabilities. The same numerical model and simulation methodology, with some more details, were discussed in Parts 1 and 2. It is noteworthy that, throughout the paper, the evolution of vorticity has been explained in terms of lobes, while the evolution of density has been explained in terms of blobs.

### 3. Simulation results

The total density is  $\rho_d = \rho_{d0} + \rho_{d1}$ . Here,  $\rho_{d0}$  is the background density. The net Gaussian density inhomogeneity is given by

$$\rho_{d1} = \rho'_{d1} + \rho'_{d2} = \rho'_{01} e^{-r_1^2/a_{c1}^2} + \rho'_{02} e^{-r_2^2/a_{c2}^2}. \quad (3.1)$$

Here,  $r_1^2 = (x - x_{01})^2 + (y - y_{01})^2$  and  $r_2^2 = (x - x_{02})^2 + (y - y_{02})^2$ . The parameters  $a_{c1}$  and  $a_{c2}$  are the initial radii of two droplets/bubbles. The separation between two droplets/bubbles is given by a distance  $d = x_{c2} - x_{c1}$ . During the numerical simulations,  $\rho_{d0} = 5$ ,  $a_{c1} = a_{c2} = a_c = 2$  are kept constant. As a result, both the droplets/bubbles exhibit spatial symmetry. A system of length  $lx = ly = 48\pi$  units with  $512 \times 512$  grid points in both the  $x$  and  $y$  axes has been taken into consideration. The system ranges from  $-24\pi$  to  $24\pi$  units along the  $x$ - and  $y$ -axes.

#### 3.1. A pair of falling droplets

Prior to providing simulation findings, it would be beneficial to have some basic qualitative understanding of the droplet–droplet dynamics. The vorticity equation (2.11) for an

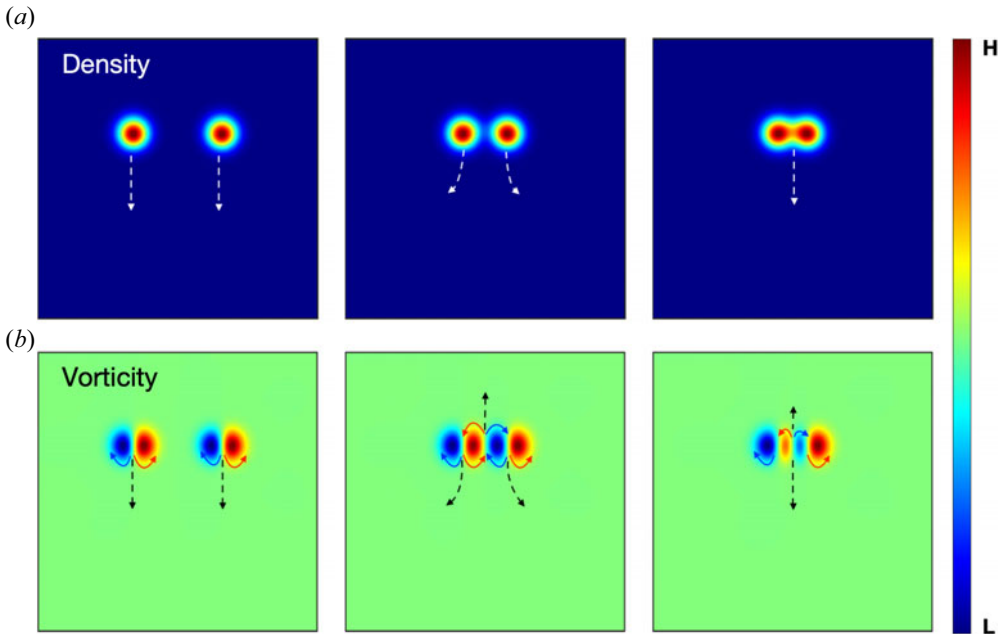


FIGURE 1. A schematic diagram of a pair of droplets placed side by side in a row. The spacing between droplets decreases from left to right: (a) the density; and (b) the vorticity profile. The net propagation is indicated by the dotted arrows in (a,b) and the curved solid arrows represent the direction of rotation of the lobes in (b). In the colour bar, The high-density region in the colour bar is represented by the abbreviation  $H$ , and the low-density/vorticity region is represented by the letter  $L$ .

inviscid flow ( $\eta = \tau_m = 0$ ) using (3.1) becomes

$$\frac{\partial \xi_z}{\partial t} + (\mathbf{v}_d \cdot \nabla) \xi_z = \frac{2g}{\rho_{d0}} (x - x_{c1}) \rho'_{d1} + \frac{2g}{\rho_{d0}} (x - x_{c2}) \rho'_{d2}. \quad (3.2)$$

In this equation, the net vorticity of two droplets is represented by the right-hand side. Both terms describe falling dipolar vorticities under the action of gravity, each has two counter-rotating (or unlike-sign) lobes.

Figure 1(a) shows the schematic profiles of two droplet densities positioned horizontally. For this configuration, figure 1(b) displays the corresponding vorticities using (3.2). The curved solid arrows over the lobes represent their direction of rotation, while net propagation is indicated by the vertical and curved dotted arrows. In this schematic figure, the spacing between a two droplets decreases from left to right. Let us first discuss the case where the two droplets are widely spaced (left-top snapshot). The left-bottom snapshot depicts the corresponding counter-rotating vorticity lobes of each droplet. Here, the left lobe rotates clockwise while the right one rotates anti-clockwise, resulting in a vertical downward motion (indicated by the vertical downward dotted arrow). Due to the large spacing between them, there is essentially no contact between these two falling droplets; hence, gravity would mostly control their dynamics, just like in the individual examples.

On the other hand, reducing the separation distance (refer to the remaining panels from left to right) enhances the possibility of vorticity pairing through the counter-rotating inner lobes. This decreasing distance between two inner lobes, where the left lobe rotates anti-clockwise while the right one rotates clockwise, induces a new dipolar structure with



vertical upward motion, as seen by the vertical dotted arrow in the middle snapshot of the bottom row. At the same time, these inner lobes pair with the outer lobes, which results in downward motion. The vorticity evolution (as demonstrated by the simulation results) makes evident that, along the direction of gravity, the inner lobes compress and elongate in shape in comparison with the outer ones. As a result, both droplets begin to move apart by following a curved trajectory with an outward curvature instead of vertical fall. The curvature of this trajectory is determined to be proportional to the pairing of the vorticity lobes until they overlap. In the right snapshots from top and bottom rows, since the two droplets are nearly in contact with one another, the overlap of two opposite-sign inner lobes eliminates each other's effects. As a result, the dipolar structure falls as one unit. This explanation makes clear that the competition between the vertical fall of two dipolar vorticities due to gravity and the interaction created by the pairing of inner vorticity lobes governs the overall dynamics. Under the influence of gravity, the dynamics described above is especially valid for an inviscid fluid.

In VE fluids, the vorticity equation (2.7) includes an extra term  $\nabla \times \psi / \rho_d$  on the right-hand side of (3.2) in addition to the gravity term. This term refers to the TS waves that excite in the medium from the rotating lobes. The speed of these waves ( $\sqrt{\eta / \rho_d \tau_m}$ ) is proportional to the coupling strength ( $\eta / \tau_m$ ) of the medium. The ensuing subsections will provide a detailed visualization of the droplet–droplet dynamics using the numerical simulations.

For simulations, both droplets ( $\rho'_{01} = \rho'_{02} = 0.5$ ) are placed side by side in a row at the same height,  $(y_{01}, y_{02}) = (8\pi, 8\pi)$ . Three spacings between two droplets are simulated: widely spaced ( $d = 24 \gg 2a_c$ ), medium spaced ( $d = 6 > 2a_c$ ) and closely spaced ( $d = 4 = 2a_c$ ), as cases (i), (ii) and (iii), respectively. For each case, the effect of the VE nature on the droplet–droplet interactions has been introduced by varying the coupling strength of the medium as mild–strong ( $\eta = 2.5, \tau_m = 20$ ) and strong ( $\eta = 2.5, \tau_m = 10$ ).

### 3.1.1. Widely spaced ( $d = 24 \gg 2a_c; a_c = 2$ )

Here, both the droplets  $(x_{c1}, x_{c2}) = (-12, 12)$  are initially separated from one another by a considerable distance ( $d = 24 \gg 2a_c; a_{c1} = a_{c2} = a_c = 2$ ), with no overlap between the inner lobes of vorticities. Let us first examine the dynamics of this pair of droplets falling side by side in an inviscid HD fluid. Since there is no dissipation or source term except gravity, the combined evolution of each droplet is supposed to be similar to an individual one. The dynamics of an individual falling droplet was covered in Part 1 (see figure 14). In an HD system, the stages that occur when an individual droplet falls are as follows: the density blobs, which were initially circular, take on crescent shapes due to gravity. Further, as time goes on, each droplet blob splits into two separate density blobs, or each droplet takes the dipolar form. These dipolar structures fall downward as a single entity and leave behind a wake-like structure in the background fluid. The time evolution of the combined density profile for both droplets in figure 2(a) makes these facts quite visible. The vorticity progression in figure 2(b) demonstrates the reason behind the falling droplet. At the onset of the simulation, the buoyant forces are induced in the form of dipolar vorticities for each droplet, each with two counter-rotating lobes. As a consequence, as was covered in more detail above through the schematic diagram in figure 1, the droplet goes vertically downward.

Next, in SCDPs, in addition to the falling trajectory, each rotating vorticity lobe emits the shear waves into the ambient fluid at a speed that is proportional to the medium's coupling strength ( $\eta / \tau_m$ ). Stated differently, a medium possessing a higher coupling strength would be able to sustain the quicker TS waves. Lobes spread more quickly as a consequence of the quicker wave's ability to cover more distance in the same amount of time. In the

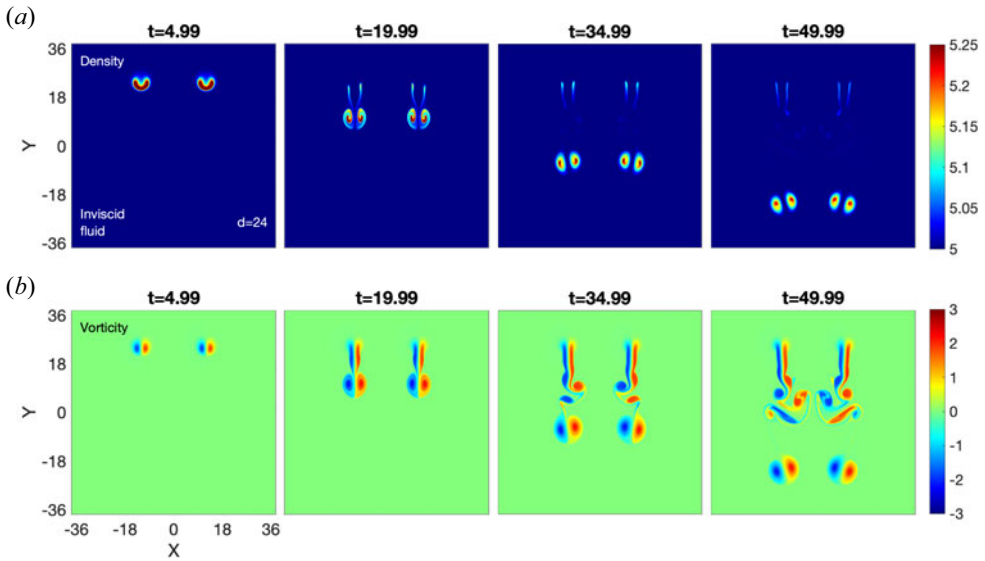


FIGURE 2. Hydrodynamic inviscid fluid. Time evolution of two widely separated droplets' density (a) (the colour bar designates the density) and vorticity (b) (the colour bar shows the vorticity) in an inviscid fluid ( $d \gg 2a_c$ ), separated by distance  $d = 24$  units. Both droplets have a nearly independent dynamics and fall the same as the individual ones.

following section, assuming a fixed viscosity  $\eta = 2.5$ , the elastic factor  $\tau_m$  solely modifies the coupling strength.

Let us start with a mild–strong VE fluid, with coupling parameter values of  $\eta = 2.5$  and  $\tau_m = 20$ . This medium supports the emission of shear waves with the phase velocity  $v_p = \sqrt{\eta/\rho_{d0}\tau_m} = 0.158$  into the surrounding fluid from both lobes. For this medium, the density evolution is depicted in figure 3. Similar to the HD scenario (figure 2a), both of the circular density blobs in this instance first take on crescent shapes before splitting into two distinct blobs of density. Panels, up to  $t = 15.48$ , of figure 3 clearly display this. Further, as time goes on (from  $t = 32.77$  to  $t = 137.44$ ), the inner blobs come close and start moving in a vertical upward direction as a single entity, while the outer start to fall at a slower rate. The reason for this different dynamics can be understood from the vorticity progression in figure 4.

In figure 4, the panels at  $t = 32.77$  and  $t = 110.13$  clearly depict the shear waves originating from each vorticity lobe. Shear waves cause the counter-rotating lobes to begin pressing against one another perpendicular to the fall of the overall structure. Consequently, the lobes gradually separate and the inner lobes get pinched in between the outer lobes. The outcome is closer proximity between the inner counter-rotating lobes and greater separation between the outer lobes since these are free to move away. The closeness of the inner lobes, the left lobe rotates anti-clockwise and the right one clockwise, produces a new dipolar structure that is characterized by vertical upward motion. The leading (waves emitting from the outer lobes in the outer side) and pushing (waves emitting from the inner lobes) shear waves make the outer lobes propagate outward, which is perpendicular to the original propagation direction. In addition, the strength of lobes/blobs is significantly diminished by the shear wave emission, which has been discussed by Dharodi *et al.* (2016) and Dharodi & Kostadinova (2024). These all contribute to slowing the fall of outer blobs. Here, it should also be highlighted that the shear waves



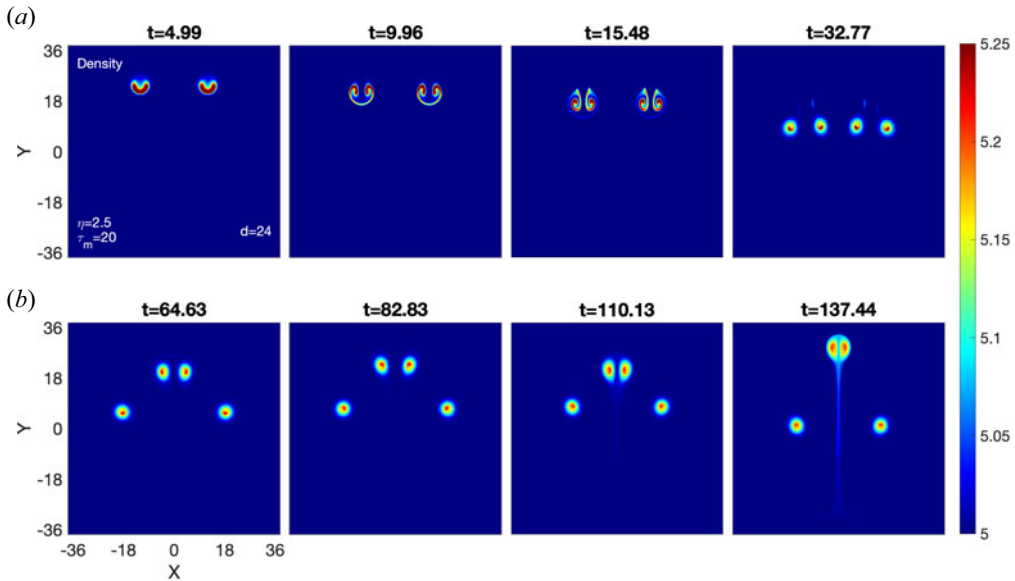


FIGURE 3. Two widely separated droplets falling side by side over time in a SCDP/VE fluid with  $\eta = 2.5$  and  $\tau_m = 20$ . The colour bar indicates the density, which is common for all the panels. Unlike a HD fluid (see [figure 2](#)), it has been found that shear waves facilitate the pairing between two droplets.

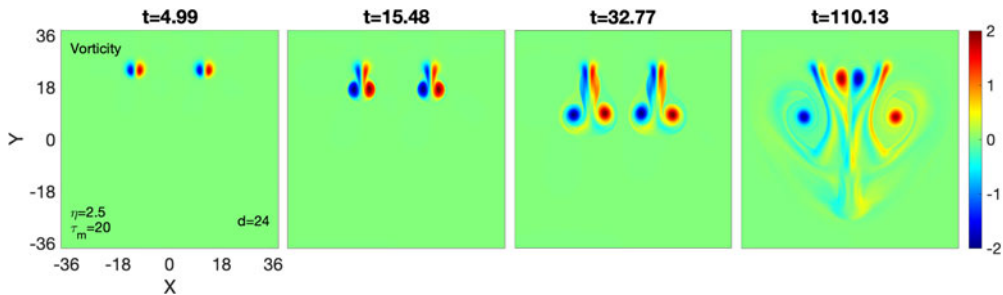


FIGURE 4. The time evolution vorticity of two widely separated droplets falling side by side in a SCDP/VE fluid with  $\eta = 2.5$  and  $\tau_m = 20$  (see [figure 3](#) for the corresponding density evolution).

have a greater effect on the inner blobs/lobes than the outside ones. As a result, the inner lobes/blobs have less strength and radial symmetry than the outside ones.

Next, for the strong coupling strength  $\eta = 2.5$ ;  $\tau_m = 10$ , [figure 5](#) depicts the evolution of density, and [figure 6](#) portrays the evolution of vorticity. Similar to the preceding example ([figure 3](#)), the inner blobs in [figure 5](#) come close to each other and begin to move in a vertical upward direction as a single entity. But, as time goes on, unlike the previous example, this inner pair suddenly starts moving in a downward direction. Eventually, the inner blobs deform into filament shapes around the upward-moving outer blobs. This is distinctly observed in panels from  $t = 64.90$  to  $t = 189.69$  of [figure 5](#).

[Figure 6](#) shows the evolution of vorticity corresponding to the density evolution in [figure 5](#). Here, the shear waves move at a phase velocity  $v_p = \sqrt{\eta/\rho_{d0}\tau_m} = 0.224$ , which is greater than the above simulated scenario. The quicker-emerging waves that remove

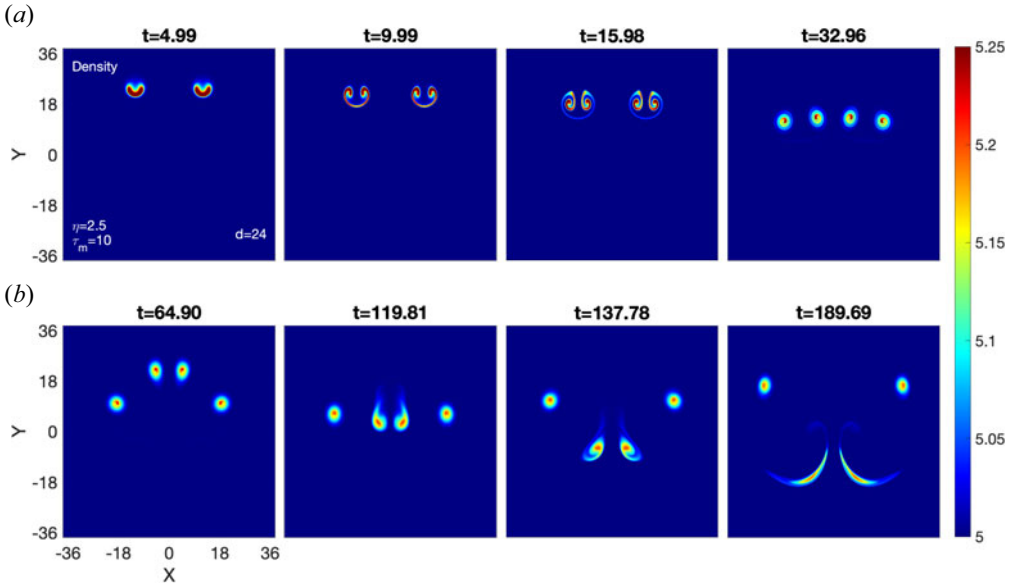


FIGURE 5. In a SCDP/VE fluid with  $\eta = 2.5$ ;  $\tau_m = 10$ , two widely separated droplets gradually fall side by side.

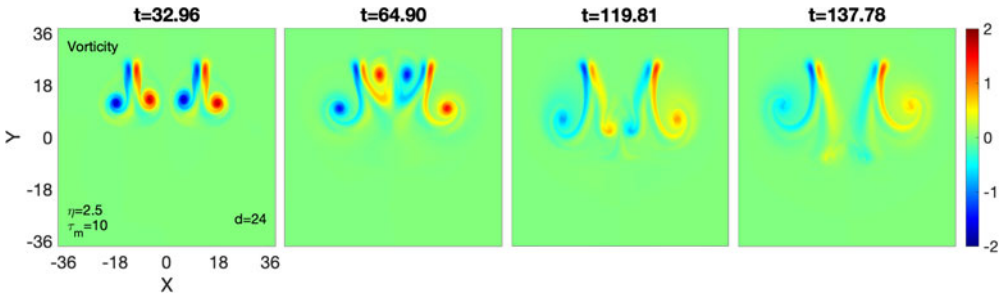


FIGURE 6. The evolution vorticity of two widely separated droplets falls side by side over time in a SCDP/VE fluid with  $\eta = 2.5$  and  $\tau_m = 10$  (see figure 5 for the corresponding density evolution).

energy from the lobes at a faster rate that results in the lobes decaying ultimately lead to its disappearance. This means the influence of rotation of the lobes is reduced more quickly. Consequently, the upward-moving inner blob pair begins to fill the gravitational supremacy and suddenly starts moving in a downward direction. Since the outer lobes are less affected by the emerging waves, they are supposed to remain symmetric and survive for a longer time. This results in the inner lobes spiralling around the rotating outer lobes.

### 3.1.2. Medium spaced ( $d = 6 > 2a_c, a_c = 2$ )

Here, both the droplets  $(x_{c1}, x_{c2}) = (-3, 3)$  are initially separated from one another by a distance ( $d = 6 > 2a_c, a_c = 2$ ), inner lobes of dipolar vorticities in close proximity to one another. Figure 7 shows the evolution of the density profile for this arrangement in an inviscid HD fluid. Similar to the previous cases, after the crescent shapes, each density blob splits into two distinct blobs. However, because there is less space between blobs, the inner blobs become more compressed and take on an elongated shape along the direction

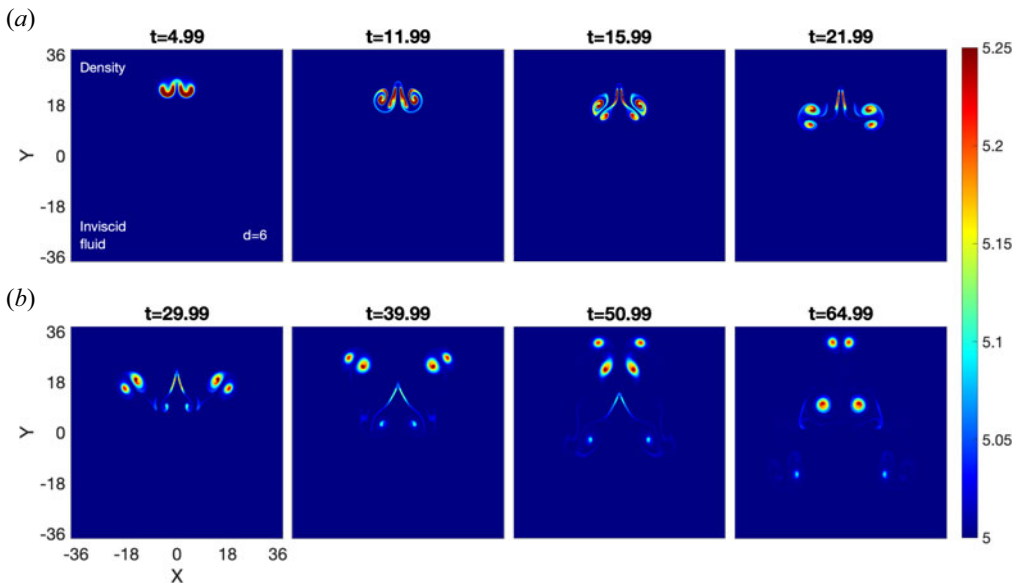


FIGURE 7. Time evolution of the density of two medium-spaced droplets separated by  $d = 6$  units in an inviscid fluid.

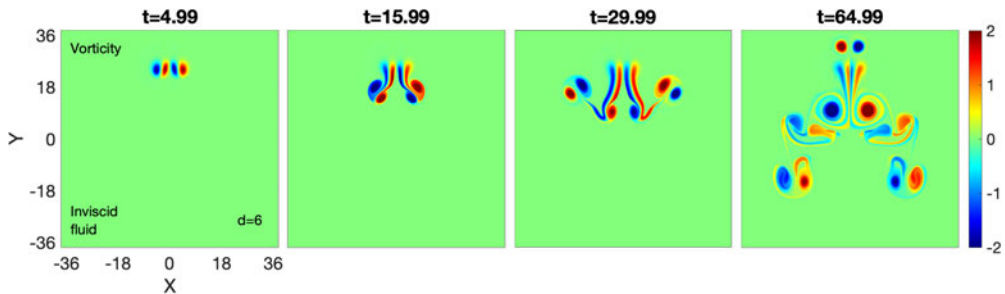


FIGURE 8. Time evolution of the vorticity of two medium-spaced droplets in an inviscid fluid (see [figure 7](#) for the corresponding density evolution).

of gravity. Under the influence of gravity, as the inner blobs propagate downward, leaving behind a wake-like structure in the background fluid, their strength gets reduced more than the outer blobs. This results two new dipoles of unequal strength blobs. As a result, they propagate apart from one another and orthogonally to the original propagation direction. This makes the dipoles exhibit circular motion. The collision between the dipoles takes place, which results in the exchange of blobs. Now the outer blobs start propagating in the same direction as gravity and the inner in the opposite direction to gravity. During this period, the wake-like structure begins to travel downward under the force of gravity, further dividing into more dipolar blobs.

[Figure 8](#) shows the evolution vorticity corresponding to the density evolution in [figure 7](#). For the main two dipoles, the inner weaker lobes try to rotate around the stronger outer lobe, that causes the blobs/lobes to move away from one another in an orthogonal direction to the original propagation direction. Likewise, lobe formation occurs with wake-like structures.

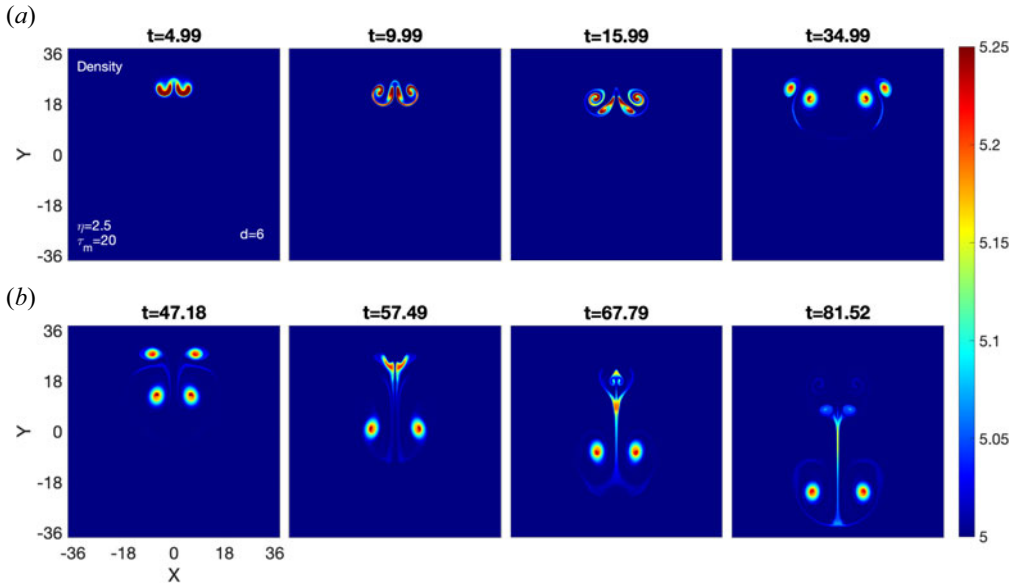


FIGURE 9. Two widely separated droplets falling side by side over time in a SCDP/VE fluid with  $\eta = 2.5$  and  $\tau_m = 20$ . The colour bar indicates the density, which is common for all the panels.

Figure 9 shows the evolution of same density configuration for the SCDP/VE case ( $\eta = 2.5$ ;  $\tau_m = 20$ ). Similar to the HD scenario (figure 7, both of the circular density blobs transform into two new dipoles of unequal strength blobs and exhibit a circular motion. The collision between the dipoles results in the exchange of blobs. But, here, both the outer and inner blobs start move downward along the direction of gravity. Next, to understand this dynamics, let us discuss the vorticity progression.

Figure 10 shows the evolution vorticity corresponding to the density evolution in figure 9. This medium supports the shear waves moving with the phase velocity  $v_p = \sqrt{\eta/\rho_{d0}\tau_m} = 0.158$ . The inner lobes are compressed in between the outer lobes by the shear waves that emanate from each rotating lobe. As a result, both dipoles split into two new dipoles, which move in a circle, with the weaker inner lobe trying to spin around the stronger outer lobe. The collision between the dipoles results in the exchange of lobes. The dipolar structure formed due to the outer (stronger) lobes continues to fall under gravity. At the time, the dipolar structure formed from the inner (weaker) lobes is supposed to travel in an upward direction, but this structure is engulfed by the shear waves, which behave like outer lobes for weaker lobes. Once again, this new arrangement produced two dipolar structures with unequal strength lobes that moved in a circle and collided. As before, this configuration created two dipolar structures of unequal lobes which performed a circular motion.

Next, figure 11 shows the evolution of density for the strong coupling strength  $\eta = 2.5$ ;  $\tau_m = 10$ , and figure 12 shows the evolution of vorticity. Similar to the preceding example (figure 9), the two new dipoles of unequal strength blobs exhibit a circular motion in figure 11. Unlike the previous example, the inner blobs deform into filament shapes around the outer blobs. This is distinctly shown in panels from  $t = 47.21$  to  $t = 81.28$  of figure 11.

Figure 12 shows the evolution of vorticity corresponding to the density evolution in figure 11. Here, the shear waves move at a phase velocity  $v_p = \sqrt{\eta/\rho_{d0}\tau_m} = 0.224$ , which

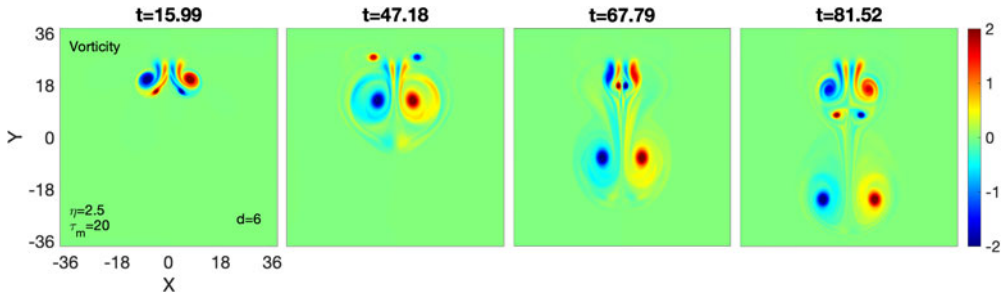


FIGURE 10. The time evolution vorticity of two medium separated droplets falling side by side in a SCDP/VE fluid with  $\eta = 2.5$  and  $\tau_m = 20$  (see figure 9 for the corresponding density evolution).

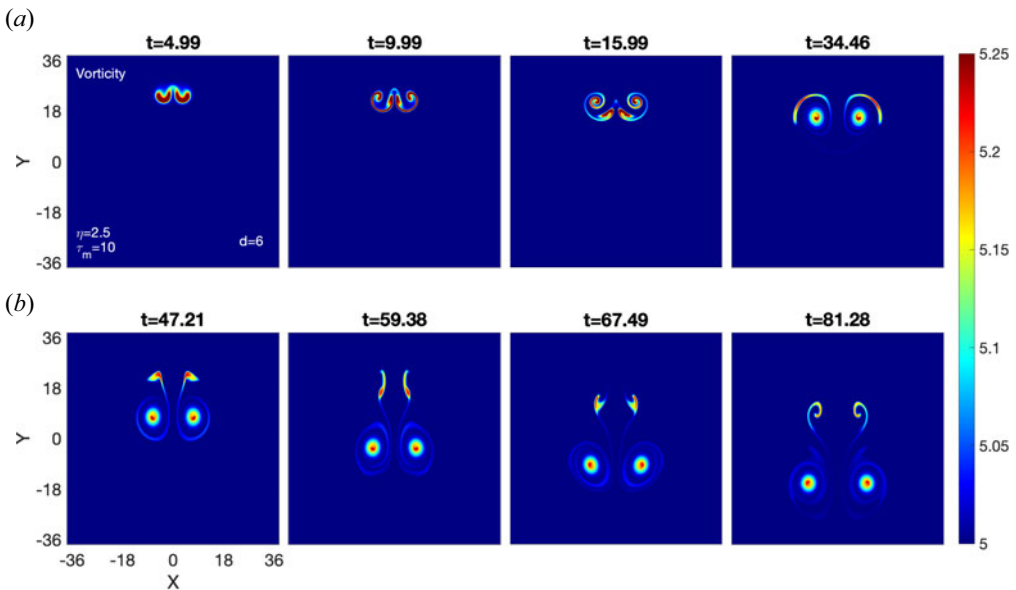


FIGURE 11. Two widely separated droplets falling side by side over time in a SCDP/VE fluid with  $\eta = 2.5$  and  $\tau_m = 10$ . The colour bar indicates the density, which is common for all the panels.

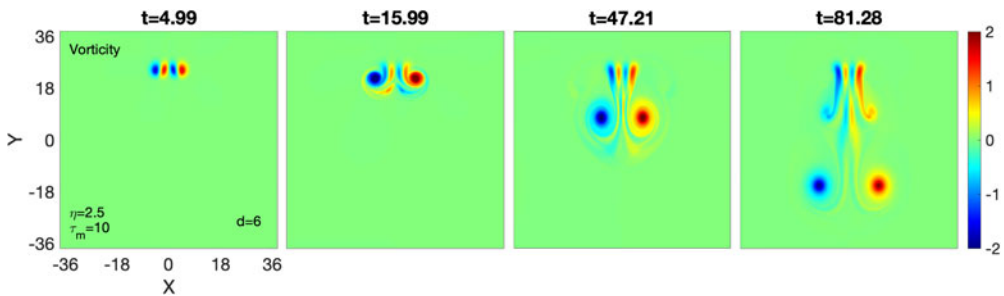


FIGURE 12. The time evolution vorticity of two medium separated droplets falling side by side in a SCDP/VE fluid with  $\eta = 2.5$  and  $\tau_m = 10$  (see figure 11 for the corresponding density evolution).

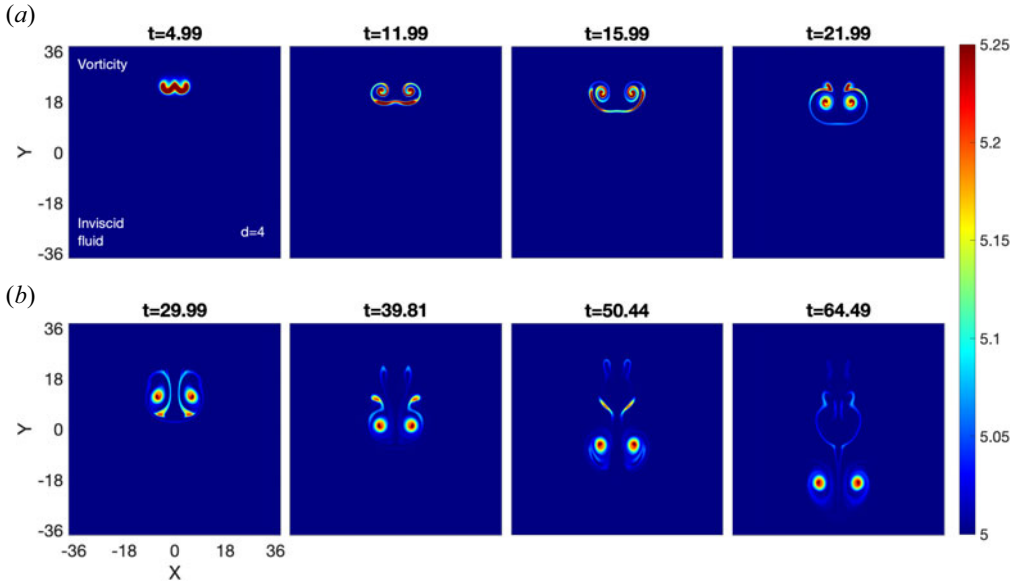


FIGURE 13. Time evolution of the density of two closely spaced droplets separated by  $d = 4$  units in an inviscid fluid.

is greater than the above simulated scenario. Compared with the previous case, here, due to the quicker-emerging waves, the weaker inner blobs notice more compression and transform into a spiral form around the outer (stronger) lobes at an earlier time. Thus, under the influence of gravity, only the outer lobe pair falls as a single entity.

### 3.1.3. Closely spaced ( $d \approx 2a_c$ )

To begin with, the droplet ( $x_{c1} = -2$ ) and bubble ( $x_{c2} = 2$ ) are placed close enough ( $d = 4 \approx 2a_c$ ) that both of the like-sign inner lobes of vorticities almost overlap with each other. Figure 13 shows the evolution of the density profile for this arrangement in an inviscid HD fluid. At the beginning of the simulation, the density produces a double-well-type structure, or ‘w’. Over time, the central bump of this structure spirals around its rotating edges. This process keeps going while the dipole (outer lobes) falls because of gravity.

Figure 14 shows the evolution vorticity corresponding to the density evolution in figure 13. The overlap of two opposite-sign inner lobes reduces the impacts of each other. Consequently, the inner lobes merely wrap around the outer lobes, which play a major role in the creation of this dipolar structure. The inner lobes spiral around their revolving outer lobes throughout time. This process continues with the dipole falling because of gravity.

Figure 15(a) shows the evolution of same density configuration for the SCDP/VE case ( $\eta = 2.5$ ;  $\tau_m = 20$ ). Similar to the HD scenario (figure 13), during the process of the dipole falling, the central bump of the double-well or ‘w’-type density profile spirals around its rotating edges. However, compared with the HD case, the wake-type structure is diminished, the lobes are better separated and the vertical upward motion gets reduced. These different observations in this VE fluid compared with a basic HD fluid are because the VE fluid favours the emission of waves from individual lobes.

A new VE fluid with  $\eta = 2.5$  and  $\tau_m = 10$  is simulated in figure 16. This medium supports the shear waves moving at a phase velocity  $v_p = \sqrt{\eta/\rho_{d0}\tau_m} = 0.224$ , which is greater than the above simulated scenario ( $v_p = \sqrt{\eta/\rho_{d0}\tau_m} = 0.158$ ; see figure 15).



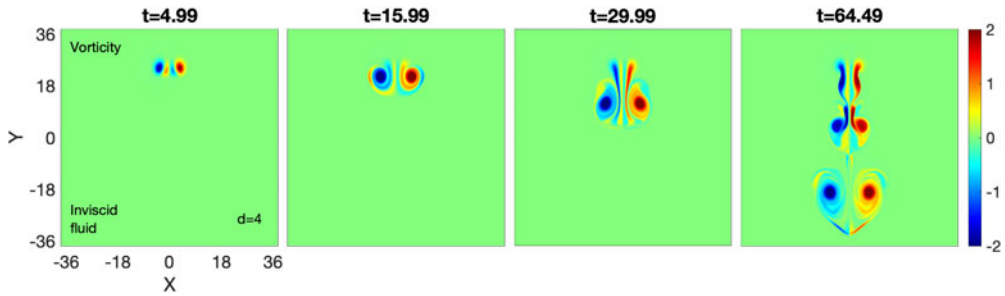


FIGURE 14. Time evolution of the vorticity of two closely spaced droplets in an inviscid fluid (see figure 13 for the corresponding density evolution).

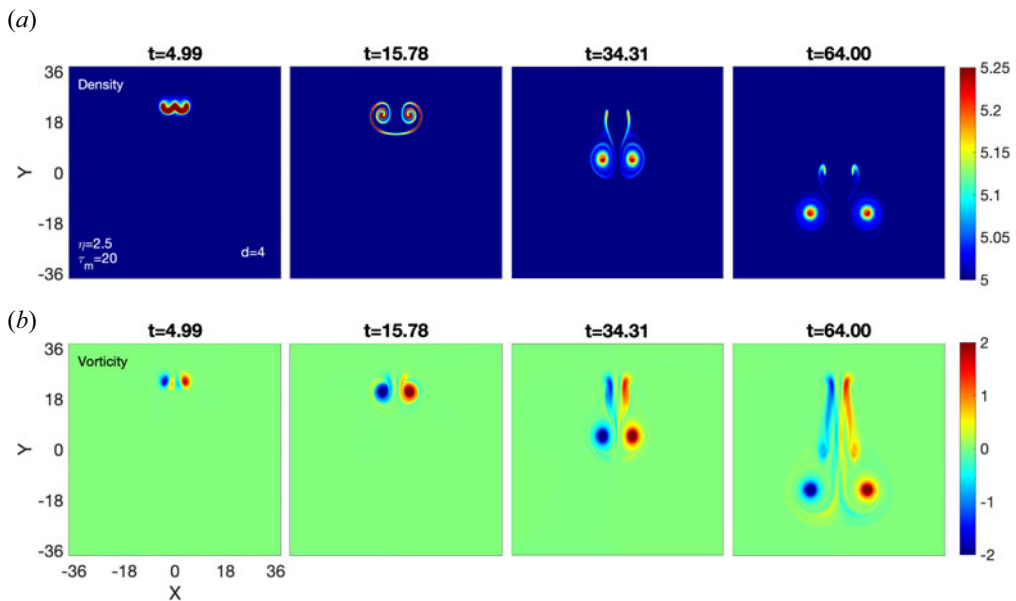


FIGURE 15. Time evolution of closely spaced droplet–droplet density (a) and vorticity (b) in a SCDP/VE fluid with  $\eta = 2.5$  and  $\tau_m = 20$ .

The faster shear waves (or the higher coupling strength) result in slower lobe vertical propagation and greater horizontal spacing between the blobs. This can be observed by the comparison analysis of the two VE fluids.

### 3.2. A pair of rising bubbles

For the rising bubbles, the initial density profile is  $\rho'_{01} = \rho'_{02} = -0.5$ . In Part 1, a rising bubble and a falling droplet have been studied independently. It is found that a rising bubble is analogous to the falling droplet process. Similarly, in the present study, in each of the three cases, it is observed that the behaviour of two falling droplets is the same as the behaviour of two rising bubbles. Thus, the only case covered here is one in which two bubbles are medium spaced ( $d = 6 > 2a_c$ ), where  $(x_{c1}, x_{c2}) = (-3, 3)$  and  $(y_{01}, y_{02}) = (-8\pi, -8\pi)$ . Figure 17 shows this density configuration for the SCDP/VE case ( $\eta = 2.5$ ;  $\tau_m = 20$ ). Here, the two circular density blobs change into two new dipoles of unequal strength. These dipoles exhibit a circular motion and then a collision results in

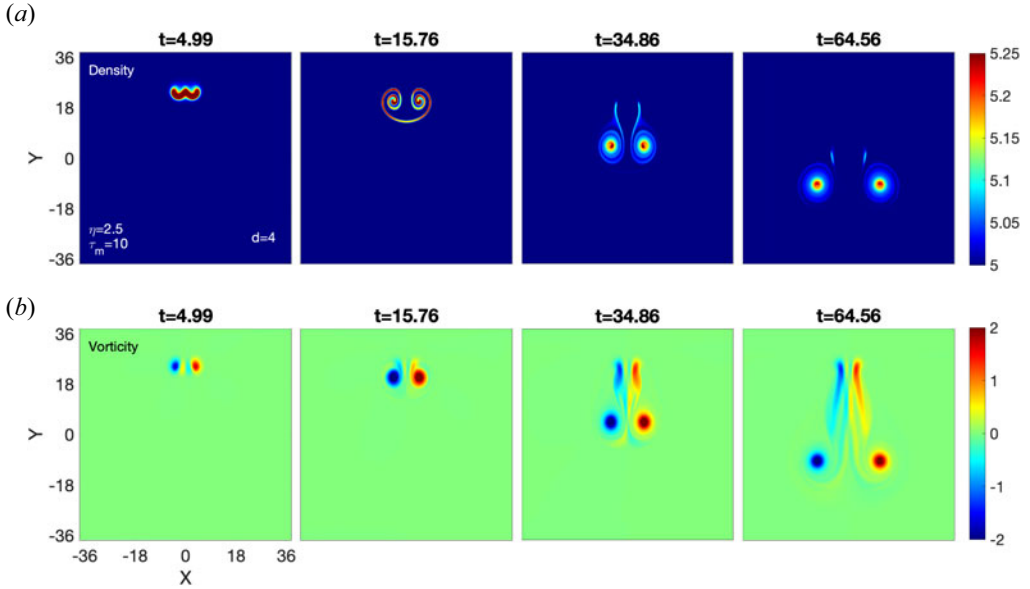


FIGURE 16. Time evolution of closely spaced droplet–droplet density (a) and vorticity (b) in a SCDP/VE fluid with  $\eta = 2.5$  and  $\tau_m = 10$ .

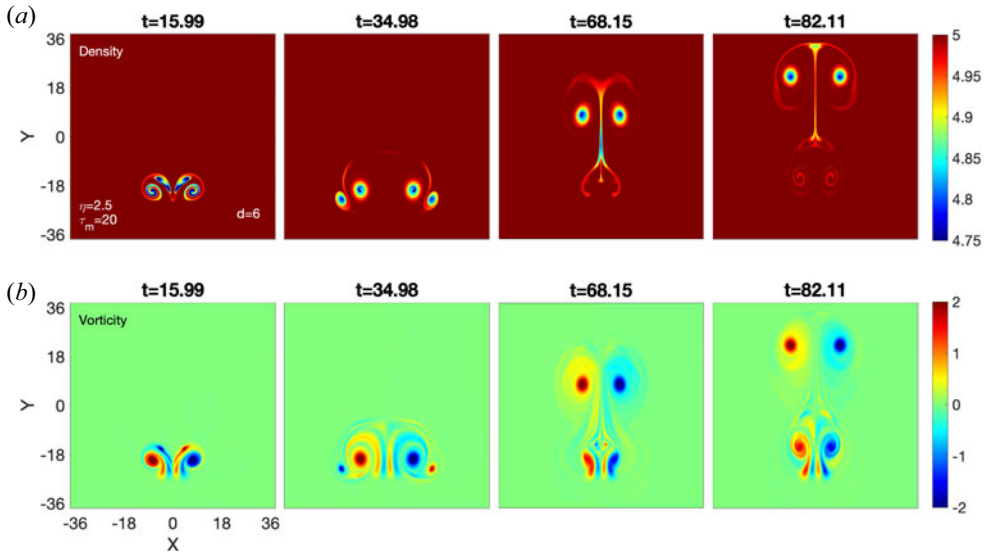


FIGURE 17. Time evolution of medium-spaced bubble–bubble density (a) and vorticity (b) in a SCDP/VE fluid with  $\eta = 2.5$  and  $\tau_m = 20$ .

the exchange of blobs. Both the outer and inner blobs start moving upward in the opposite direction to gravity. A comparison of figures 17(a) and 9 demonstrates that the processes of two rising bubbles and two falling droplets are identical.

Figure 17(b) shows the evolution vorticity corresponding to the density evolution in figure 17(a). This medium favours the shear waves moving with the phase velocity  $v_p = \sqrt{\eta/\rho_{d0}\tau_m} = 0.158$ . Due to the emerging shear waves from each lobe, two new dipoles

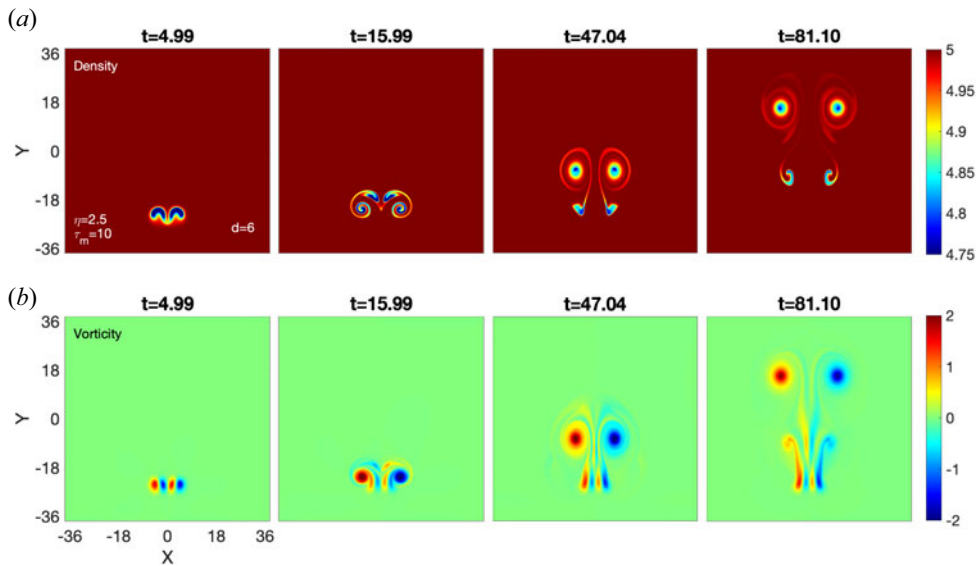


FIGURE 18. Time evolution of medium-spaced bubble–bubble density (a) and vorticity (b) in a SCDP/VE fluid with  $\eta = 2.5$  and  $\tau_m = 10$ .

are formed, which move in a circle. The weaker inner lobe attempting to rotate around the stronger outer lobe is what drives this circulation motion. The collision between the dipoles results in the exchange of lobes. The outer (stronger) lobes continue to rise as a dipolar structure. The dipolar structure formed from the inner (weaker) lobes is swallowed by the shear waves, which behave like outer lobes for weaker lobes. Once again, this new configuration results in two dipolar structures with different lobe strengths that move in a circle and collide. The evolutions of vorticity of two rising bubbles and two falling droplets are identical, as can be shown by comparing figures 17(b) and 10.

Next, figure 18(a) shows the evolution of density for the strong coupling strength  $\eta = 2.5$ ;  $\tau_m = 10$ , and figure 18(b) shows the evolution of vorticity. In this case, the evolutions of vorticity/density profiles of two rising bubbles and two falling droplets are identical, as can be shown by comparing figures 18(a) and 11, and figures 18(b) and 12.

The aforementioned findings may hold significance for any plasma that exhibits density heterogeneity when subjected to shear waves. Such heterogeneity, for instance, may arise in fusion plasmas, where external forces like magnetic or electric forces might act like gravity.

#### 4. Conclusions

The main objective of this paper is to understand the homo-interactions between two droplets that are falling and two bubbles that are rising in a strongly coupled plasma medium. This medium has been considered as a VE fluid using the generalized hydrodynamic fluid model formalism. This work (Part 3) is a continuation of our earlier published work, Parts 1 and 2. The dynamics of a falling droplet and a rising bubble were examined independently in Part 1 (Dharodi & Das 2021), and the hetero- (bubble–droplet) interactions between the two were examined in Part 2 (Dharodi 2021). In order to understand the homo-interactions, a series of two-dimensional numerical simulations have been carried out. Three different spacings between two droplets are simulated: widely, medium and closely. In each case, the coupling strength has been presented as mild–strong

( $\eta = 2.5, \tau_m = 20$ ) and strong ( $\eta = 2.5, \tau_m = 10$ ). Since the behaviour of two falling droplets is similar to the behaviour of two rising bubbles, the discussion here focuses mainly on the droplet case. A few significant findings are as follows:

(i) Widely spaced

– In the case of dusty plasma, unlike the HD fluid, emerging shear waves facilitate the pairing between two falling droplets. Due to the emerging shear waves the inner lobes get pinched in between the outer lobes. The closeness of the inner lobes produces a new dipolar structure that is characterized by vertical upward motion. The outer lobes propagate outward, which is perpendicular to the original propagation direction. In a plasma with mild strong coupling strength the vertical upward motion of the inner dipole continued. But for a plasma with a strong coupling strength, the quicker-emerging waves remove energy from the lobes at a faster rate that reduces the rotating influence of the lobes more quickly. Consequently, the upward-moving inner blob pair begins to fill the gravitational supremacy and suddenly starts moving in a downward direction.

(ii) Medium spaced

– Here, the coupling between the inner lobes results in two new dipolar structures which have unequal strength lobes. These new two dipoles exhibit circular motion instead of vertical fall, where they collide with each other and exchange partners. After this, the outer lobes fall down along the direction of gravity, while the inner lobes begin to move upward against gravity. For the mild–strong coupling strength medium, similar to the HD scenario, it is observed that two new dipoles of unequal strength blobs exhibit a circular motion and exchange the blobs. But here both the outer and inner blobs start moving downward along the direction of gravity. For the strong coupling strength medium, not like the mild example, the inner blobs deform into filament shapes around the outer blobs.

(iii) Closely spaced

– The unlike-sign inner lobes of vorticities almost overlap with each other. So, under gravity, the pair of two droplets shows the downward dynamics of a single pair. In a mild coupled plasma, compared with the HD case, the wake-type structure is diminished, the lobes are better separated and the vertical upward motion gets reduced. In a strong coupled plasma, the faster shear waves result in slower lobe vertical propagation and greater horizontal spacing between the blobs.

In summary, the net dynamic is governed by the competition between the mutual attraction of two inner like-sign vorticity lobes and the forward vertical motion of dipolar vorticities (unlike-sign lobes) due to gravity. In this paper, the study of bubble–bubble/droplet–droplet interactions has been confined to a homogeneous background density medium. However, it would be exciting to extend this to a heterogeneous background density medium. The dynamics in a heterogeneous medium will get more complex due to the varying speed of shear waves with density (Dharodi 2020). Furthermore, adding compressibility to the existing model will make it more like a real system. It would be interesting to observe how the dynamics of the rising bubble or falling droplet is affected by the energy exchange between both modes and by newly developing waves.

## Acknowledgements

The author thanks Bhawana for editing assistance. This research received no specific grant from any funding agency, commercial or not-for-profit sectors.

*Editor Edward Thomas, Jr. thanks the referees for their advice in evaluating this article.*

## Declaration of interest

The author reports no conflict of interest.

## REFERENCES

- ALIABOUZAR, M., KRIPFGANS, O.D., FOWLKES, J.B. & FABIILLI, M.L. 2023 Bubble nucleation and dynamics in acoustic droplet vaporization: a review of concepts, applications, and new directions. *Z. Med. Physik.* **33** (3), 387–406.
- ARZHANNIKOV, A.V., BATAEV, V.A., BATAEV, I.A., BURDAKOV, A.V., IVANOV, I.A., IVANTSIVSKY, M.V., KUKLIN, K.N., MEKLER, K.I., ROVENSKIKH, A.F., POLOSATKIN, S.V., *et al.* 2013 Surface modification and droplet formation of tungsten under hot plasma irradiation at the GOL-3. *J. Nucl. Mater.* **438**, S677–S680.
- BORIS, J.P., LANDSBERG, A.M., ORAN, E.S. & GARDNER, J.H. 1993 LCPFCT A flux-corrected transport algorithm for solving generalized continuity equations. *Tech. Rep.* NRL Memorandum Report 93-7192, Naval Research Laboratory.
- BOUROUBA, L. & BUSH, J.W.M. 2012 Drops and bubbles in the environment. In *Handbook of Environmental Fluid Dynamics*, vol. 1, pp. 445–458. CRC.
- CHAUBEY, N. & GOREE, J. 2022a Coulomb expansion of a thin dust cloud observed experimentally under afterglow plasma conditions. *Phys. Plasmas* **29** (11).
- CHAUBEY, N. & GOREE, J. 2022b Preservation of a dust crystal as it falls in an afterglow plasma. *Front. Phys.* **10**, 879092.
- CHAUBEY, N. & GOREE, J. 2023a Controlling the charge of dust particles in a plasma afterglow by timed switching of an electrode voltage. *J. Phys. D: Appl. Phys.* **56** (37), 375202.
- CHAUBEY, N. & GOREE, J. 2023b Mitigating dust particle contamination in an afterglow plasma by controlled lifting with a dc electric field. *J. Phys. D: Appl. Phys.* **57** (10), 105201.
- CHAUBEY, N. & GOREE, J. 2024 Controlling the charge of dust particles in an afterglow by modulating the plasma power. *J. Phys. D: Appl. Phys.* **57** (20), 205202.
- CHAUBEY, N., GOREE, J., LANHAM, S.J. & KUSHNER, M.J. 2021 Positive charging of grains in an afterglow plasma is enhanced by ions drifting in an electric field. *Phys. Plasmas* **28** (10).
- CHEN, R.-H., TAN, D.S., LIN, K.-C., CHOW, L.C., GRIFFIN, A.R. & RINI, D.P. 2008 Droplet and bubble dynamics in saturated FC-72 spray cooling on a smooth surface. *Trans. ASME J. Heat Transfer* **130** (10).
- CHEN, Y.-H., CHU, H.-Y. & LIN, I. 2006 Interaction and fragmentation of pulsed laser induced microbubbles in a narrow gap. *Phys. Rev. Lett.* **96** (3), 034505.
- CHOUDHARY, M., MUKHERJEE, S. & BANDYOPADHYAY, P. 2016 Propagation characteristics of dust–acoustic waves in presence of a floating cylindrical object in the dc discharge plasma. *Phys. Plasmas* **23** (8).
- CHOUDHARY, M., MUKHERJEE, S. & BANDYOPADHYAY, P. 2017 Experimental observation of self excited co-rotating multiple vortices in a dusty plasma with inhomogeneous plasma background. *Phys. Plasmas* **24** (3).
- CHOUDHARY, M., MUKHERJEE, S. & BANDYOPADHYAY, P. 2018 Collective dynamics of large aspect ratio dusty plasma in an inhomogeneous plasma background: formation of the co-rotating vortex series. *Phys. Plasmas* **25** (2).
- CHU, H.-Y., CHIU, Y.-K., CHAN, C.-L. & LIN, I. 2003 Observation of laser-pulse-induced traveling microbubbles in dusty plasma liquids. *Phys. Rev. Lett.* **90** (7), 075004.
- CRISTINI, V. & TAN, Y.-C. 2004 Theory and numerical simulation of droplet dynamics in complex flows—a review. *Lab on a Chip* **4** (4), 257–264.

- DAS, A., DHARODI, V. & TIWARI, S. 2014 Collective dynamics in strongly coupled dusty plasma medium. *J. Plasma Phys.* **80** (6), 855–861.
- DHARODI, V. 2016 Collective phenomena in strongly coupled dusty plasma medium. PhD thesis, Homi Bhabha National Institute.
- DHARODI, V. 2020 Rotating vortices in two-dimensional inhomogeneous strongly coupled dusty plasmas: shear and spiral density waves. *Phys. Rev. E* **102** (4), 043216.
- DHARODI, V. 2021 A numerical study of gravity-driven instability in strongly coupled dusty plasma. Part 2. Hetero-interactions between a rising bubble and a falling droplet. *J. Plasma Phys.* **87** (4), 905870402.
- DHARODI, V. & DAS, A. 2021 A numerical study of gravity-driven instability in strongly coupled dusty plasma. Part 1. Rayleigh–Taylor instability and buoyancy-driven instability. *J. Plasma Phys.* **87** (2), 905870216.
- DHARODI, V. & KOSTADINOVA, E. 2023 Ring structural transitions in strongly coupled dusty plasmas. *Phys. Rev. E* **107** (5), 055208.
- DHARODI, V. & KOSTADINOVA, E. 2024 Vortex merging in strongly coupled dusty plasmas using a visco-elastic fluid model. *Phys. Plasmas* **31** (5), 053702.
- DHARODI, V., PATEL, B. & DAS, A. 2022 Kelvin–Helmholtz instability in strongly coupled dusty plasma with rotational shear flows and tracer transport. *J. Plasma Phys.* **88** (1), 905880103.
- DHARODI, V.S., DAS, A., PATEL, B.G. & KAW, P.K. 2016 Sub- and super-luminal propagation of structures satisfying Poynting-like theorem for incompressible generalized hydrodynamic fluid model depicting strongly coupled dusty plasma medium. *Phys. Plasmas* **23** (1), 013707.
- DHARODI, V.S., TIWARI, S.K. & DAS, A. 2014 Visco-elastic fluid simulations of coherent structures in strongly coupled dusty plasma medium. *Phys. Plasmas* **21** (7), 073705.
- DOLLET, B., MARMOTTANT, P. & GARBIN, V. 2019 Bubble dynamics in soft and biological matter. *Annu. Rev. Fluid Mech.* **51**, 331–355.
- DWYER, H.A. 1989 Calculations of droplet dynamics in high temperature environments. *Prog. Energy Combust. Sci.* **15** (2), 131–158.
- FENG, Y., GOREE, J. & LIU, B. 2012 Frequency-dependent shear viscosity of a liquid two-dimensional dusty plasma. *Phys. Rev. E* **85** (6), 066402.
- FRENKEL, J. 1955 *Kinetic Theory Of Liquids*. Dover Publications.
- GAUDRON, R., WARNEZ, M.T. & JOHNSEN, E. 2015 Bubble dynamics in a viscoelastic medium with nonlinear elasticity. *J. Fluid Mech.* **766**.
- IKEZI, H. 1986 Coulomb solid of small particles in plasmas. *Phys. Fluids* **29** (6), 1764–1766.
- JIA, W. & ZHU, H. 2015 Dynamics of water droplet impact and spread on soybean leaves. *Trans. ASABE* **58** (4), 1109–1016.
- KAW, P.K. 2001 Collective modes in a strongly coupled dusty plasma. *Phys. Plasmas* **8** (5), 1870–1878.
- KAW, P.K. & SEN, A. 1998 Low frequency modes in strongly coupled dusty plasmas. *Phys. Plasmas* **5** (10), 3552–3559.
- KONG, G., MIRSANI, H., BUIST, K.A., PETERS, E.A.J.F., BALTUSSEN, M.W. & KUIPERS, J.A.M. 2019 Hydrodynamic interaction of bubbles rising side-by-side in viscous liquids. *Exp. Fluids* **60** (10), 155.
- KUMAR, K., BANDYOPADHYAY, P., SINGH, S., DHARODI, V.S. & SEN, A. 2023 Kelvin–Helmholtz instability in a compressible dust fluid flow. *Sci. Rep.* **13** (1), 3979.
- LEONG, F.Y. & LE, D.-V. 2020 Droplet dynamics on viscoelastic soft substrate: toward coalescence control. *Phys. Fluids* **32** (6), 062102.
- MELZER, A., NUNOMURA, S., SAMSONOV, D., MA, Z.W. & GOREE, J. 2000 Laser-excited Mach cones in a dusty plasma crystal. *Phys. Rev. E* **62** (3), 4162.
- MERLINO, R.L. & GOREE, J.A. 2004 Dusty plasmas in the laboratory, industry, and space. *Phys. Today* **57** (7), 32–38.
- MOGHHTADERNEJAD, S., LEE, C. & JADIDI, M. 2020 An introduction of droplet impact dynamics to engineering students. *Fluids* **5** (3), 107.
- MOKHTARZADEH-DEHGHAN, M.R. & EL-SHIRBINI, A.A. 1985 Dynamics of two-phase bubble-droplets in immiscible liquids. *Wärme-und Stoffübertragung* **19** (1), 53–59.



- NING, W., LAI, J., KRUSZELNICKI, J., FOSTER, J.E., DAI, D. & KUSHNER, M.J. 2021 Propagation of positive discharges in an air bubble having an embedded water droplet. *Plasma Sources Sci. Technol.* **30** (1), 015005.
- NUNOMURA, S., SAMSONOV, D. & GOREE, J. 2000 Transverse waves in a two-dimensional screened-coulomb crystal (dusty plasma). *Phys. Rev. Lett.* **84** (22), 5141.
- OINUMA, G., NAYAK, G., DU, Y. & BRUGGEMAN, P.J. 2020 Controlled plasma–droplet interactions: a quantitative study of oh transfer in plasma–liquid interaction. *Plasma Sources Sci. Technol.* **29** (9), 095002.
- OU, W., BROCHARD, F. & MORGAN, T.W. 2021 Bubble formation in liquid Sn under different plasma loading conditions leading to droplet ejection. *Nucl. Fusion* **61** (6), 066030.
- PEETERS, F.M. & WU, X. 1987 Wigner crystal of a screened-coulomb-interaction colloidal system in two dimensions. *Phys. Rev. A* **35** (7), 3109.
- PRAMANIK, J., PRASAD, G., SEN, A. & KAW, P.K. 2002 Experimental observations of transverse shear waves in strongly coupled dusty plasmas. *Phys. Rev. Lett.* **88** (17), 175001.
- RAMKORUN, B., CHANDRASEKHAR, G., RANGARI, V., THAKUR, S.C., COMES, R.B. & THOMAS, E. JR. 2024a Comparing growth of titania and carbonaceous dusty nanoparticles in weakly magnetised capacitively coupled plasmas. *Plasma Sources Sci. Technol.* [arXiv:2402.00951](https://arxiv.org/abs/2402.00951).
- RAMKORUN, B., JAIN, S., TABA, A., MAHJOURI-SAMANI, M., MILLER, M.E., THAKUR, S.C., THOMAS, E. & COMES, R.B. 2024b Introducing dusty plasma particle growth of nanospherical titanium dioxide. *Appl. Phys. Lett.* **124** (14).
- SCHMIDT, P., ZWICKNAGEL, G., REINHARD, P.-G. & TOEPFFER, C. 1997 Longitudinal and transversal collective modes in strongly correlated plasmas. *Phys. Rev. E* **56** (6), 7310.
- SCHWABE, M., RUBIN-ZUZIC, M., ZHDANOV, S., IVLEV, A.V., THOMAS, H.M. & MORFILL, G.E. 2009 Formation of bubbles, blobs, and surface cusps in complex plasmas. *Phys. Rev. Lett.* **102** (25), 255005.
- SHEW, W.L. & PINTON, J.-F. 2006 Viscoelastic effects on the dynamics of a rising bubble. *J. Stat. Mech.* **2006** (01), P01009.
- SHUKLA, P.K. & MAMUN, A.A. 2015 *Introduction to Dusty Plasma Physics*. CRC.
- STENZEL, R.L. & URRUTIA, J.M. 2012a Oscillating plasma bubbles. I. Basic properties and instabilities. *Phys. Plasmas* **19** (8).
- STENZEL, R.L. & URRUTIA, J.M. 2012b Oscillating plasma bubbles. II. Pulsed experiments. *Phys. Plasmas* **19** (8).
- STENZEL, R.L. & URRUTIA, J.M. 2012c Oscillating plasma bubbles. III. Internal electron sources and sinks. *Phys. Plasmas* **19** (8).
- STENZEL, R.L. & URRUTIA, J.M. 2012d Oscillating plasma bubbles. IV. Grid, gradients and geometry. *Phys. Plasmas* **19**, 082108.
- SWARZTRAUBER, P., SWEET, R. & ADAMS, J.C. 1999 *FISHPACK: Efficient FORTRAN Subprograms for the Solution of Elliptic Partial Differential Equations*. UCAR Publication.
- TABOR, R.F., WU, C., LOCKIE, H., MANICA, R., CHAN, D.Y.C., GRIESER, F. & DAGASTINE, R.R. 2011 Homo- and hetero-interactions between air bubbles and oil droplets measured by atomic force microscopy. *Soft Matt.* **7** (19), 8977–8983.
- TACHIBANA, K., TAKEKATA, Y., MIZUMOTO, Y., MOTOMURA, H. & JINNO, M. 2011 Analysis of a pulsed discharge within single bubbles in water under synchronized conditions. *Plasma Sources Sci. Technol.* **20** (3), 034005.
- TENG, L.-W., TSAI, C.-Y., TSENG, Y.-P. & LIN, I. 2008 Micro dynamics of pulsed laser induced bubbles in dusty plasma liquids. In *AIP Conference Proceedings*, vol. 1041, pp. 333–334. American Institute of Physics.
- TIWARI, S., DHARODI, V., DAS, A., KAW, P. & SEN, A. 2014a Kelvin–Helmholtz instability in dusty plasma medium: fluid and particle approach. *J. Plasma Phys.* **80** (6), 817–823.
- TIWARI, S.K., DHARODI, V.S., DAS, A., PATEL, B.G. & KAW, P. 2014b Evolution of sheared flow structure in visco-elastic fluids. In *AIP Conference Proceedings*, vol. 1582, pp. 55–65. American Institute of Physics.
- TIWARI, S.K., DHARODI, V.S., DAS, A., PATEL, B.G. & KAW, P. 2015 Turbulence in strongly coupled dusty plasmas using generalized hydrodynamic description. *Phys. Plasmas* **22** (2).

- VLADIMIROV, S.V., SHEVCHENKO, P.V. & CRAMER, N.F. 1997 Vibrational modes in the dust-plasma crystal. *Phys. Rev. E* **56** (1), R74.
- WANG, B., WANG, J., YU, C., LUO, S., PENG, J., LI, N., WANG, T., JIANG, L., DONG, Z. & WANG, Y. 2023 Sustained agricultural spraying: from leaf wettability to dynamic droplet impact behavior. *Global Challenges* **7** (9), 2300007.
- WANG, G.J., SHI, J.K., REINISCH, B.W., WANG, X. & WANG, Z. 2015 Ionospheric plasma bubbles observed concurrently by multi-instruments over low-latitude station hainan. *J. Geophys. Res.: Space Phys.* **120** (3), 2288–2298.
- WANG, X., BHATTACHARJEE, A. & HU, S. 2001 Longitudinal and transverse waves in yukawa crystals. *Phys. Rev. Lett.* **86** (12), 2569.
- ZHANG, J., CHEN, L. & NI, M.-J. 2019 Vortex interactions between a pair of bubbles rising side by side in ordinary viscous liquids. *Phys. Rev. Fluids* **4** (4), 043604.
- ZHAO, L., BOUFADEL, M.C., KING, T., ROBINSON, B., GAO, F., SOCOLOFSKY, S.A. & LEE, K. 2017 Droplet and bubble formation of combined oil and gas releases in subsea blowouts. *Mar. Pollut. Bull.* **120** (1–2), 203–216.
- ZHU, X., SUI, P.C. & DJILALI, N. 2008 Three-dimensional numerical simulations of water droplet dynamics in a PEMFC gas channel. *J. Power Sources* **181** (1), 101–115.